Propeller-hull interaction beyond the propulsive factors-A case study on the performance of different propeller designs

Ocean Engineering 256 (2022) 111424

Contents lists available at ScienceDirect

Ocean Engineering

journal homepage: www.elsevier.com/locate/oceaneng

Propeller–hull interaction beyond the propulsive factors—A case study on the performance of different propeller designs

Jennie Andersson [a,*], Robert Gustafsson [b], Rikard Johansson [b], Rickard E. Bensow [a]

[a] Department of Mechanics and Maritime Sciences, Chalmers University of Technology, Göteborg, Sweden
[b] Kongsberg Maritime Hydrodynamic Research Centre, Kongsberg Maritime Sweden AB, Kristinehamn, Sweden

ARTICLE INFO

Keywords:
Hull–propulsion system interaction
Propulsive factors
RANS
Tip-unloaded propeller
Ice-classed propeller

ABSTRACT

The propulsive factors are critical for scaling of model-test data, and hence important for the final power prediction. When comparing different propulsion systems based on model-scale tests, differences in propulsive factors, and hence the propeller–hull interaction, are often not well understood. In this study the propeller–hull interaction is instead described and compared using CFD for three different propulsion systems, a tip-unloaded ice-classed propeller, an ice-classed propeller with conventional radial load distribution and a non ice-classed propeller with conventional radial load distribution. To post-process the results K_T/K_Q is evaluated for one blade around a revolution and complemented with radial distributions of the same measure. Both tip-unloaded blades and sharp leading edges suffer in-behind due to poor performance at low load. Open water performance dependency on Reynolds number reveals that ice-classed propellers are more negatively influenced by the low Reynolds numbers of self-propulsion tests. Further, it is noted that a more even radial load distribution favours a low thrust deduction factor. Since the propulsive factors to a large extent are influenced by scale-effects and also due to that their association to the observed hydrodynamics makes the commonly applied scaling procedure of them questionable, they are not considered representative for ship-scale power prediction.

1. Introduction

In ship design, model-scale testing in towing tanks and associated scaling procedures (ITTC, 2017) is still the main tool for performance prediction for final comparisons between suppliers and contractual agreements. The propeller–hull interaction, i.e. how well the propeller, hull and rudder functions as a system, rather than as separate components, is in the scaling procedure accounted for using the propulsive factors. These include variables such as thrust deduction (t), Taylor wake fraction (w_T), and relative rotative efficiency (η_R), relating the resistance of the bare hull to the resistance of the hull with working propeller in-behind and the performance of the propeller in open water to the performance behind the vessel. These propulsive factors are critical components in the scaling of the model-test data to ship-scale, and hence important for the final power prediction of the vessel.

When comparing different propulsion systems based on the model-scale tests differences in the propulsive factors are often not well understood. One such typical case is the differences in propulsive factors between the first self-propulsion tests with a stock propeller and the later tests with the design propeller. Even if the main details of the propeller are targeted to be similar, differences in terms of pitch distribution, ice class, and other properties may still be present. That the propulsive factors are not well understood is at least partly a consequence of that they aggregate several hydrodynamic differences in single numbers without any possibilities to separate the flow features contributing to the differences. In addition to that, it is generally accepted that the propulsion system performance in model-scale may be influenced by the low Reynolds number of the self-propulsion test, primarily due to laminar boundary layers and laminar to turbulent transition on the propeller blades. Differences in performance due to inconsistent Reynolds numbers of open water and self-propulsion tests may therefore also be incorporated in the propulsive factors and contribute to difficulties in understanding them, as for instance discussed by Lücke (2019) and Li et al. (2019).

Since the propulsive factors often do not reveal hydrodynamic details about the propeller–hull interaction, it is considered as a design field highly relevant for application of Computational Fluid Dynamics (CFD), where more flow details can be extracted. In addition, CFD can be applied to the system in both model and ship-scale, enabling possibilities to study potential differences between the different scales. However, in published literature on propeller–hull interaction utilizing CFD it is surprisingly common to focus on the evaluation of propulsive factors, even though CFD poses more possibilities to understand these

* Corresponding author.
E-mail address: jennie.andersson@chalmers.se (J. Andersson).

https://doi.org/10.1016/j.oceaneng.2022.111424
Received 7 May 2021; Received in revised form 10 April 2022; Accepted 24 April 2022
Available online 18 May 2022

Fig. 1. Side-view of the hull.

interactions. Studies moving beyond the traditional characterization in the form of propulsive factors can roughly be grouped into two categories: those taking an volume integral approach of the flow, such as energy balance analyses (Hally, 2019; Schuiling and van Terwisga, 2018; Andersson et al., 2018; Eslamdoost et al., 2017) and those based on surface integrals of forces on hull and propulsion system. Even though the second category is easily available, and probably the most commonly used within industry, there are only few examples published, see for instance Schuiling and Van Terwisga (2017), Liefvendahl and Bensow (2014), Bensow (2015), Voermans (2017) presenting forces and performance of the blade around a revolution.

The objective of this study is to describe and understand the interaction effects in both model- and ship-scale and thereafter evaluate to what extent the propulsive factors obtained from model testing are representative to use in the scaling procedure. Hence, a secondary objective is to present post-processing alternatives to describe interaction effects based on CFD-results. The comparison of interaction effects has been conducted on one vessel with three alternative propulsion systems, (A) a tip-unloaded ice-classed propeller, (B) an ice-classed propeller with conventional radial load distribution and (C) a non ice-classed propeller with conventional radial load distribution. The investigations will be limited to propeller–hull interaction effects at design conditions, and hence only one operating condition, the design speed of the vessel, is studied. Validation of the CFD model is conducted for system A, where model test data are available, while the comparisons between configurations are based solely on CFD-results.

This article is structured as follows: Section 2 describes the hull and the three propulsion systems. The flow solver, CFD modelling and computational grids are described in Section 3. In Section 4 the validation of the CFD models are outlined and discussed. The comparison of the different propulsion systems in terms of propeller–hull interaction and discussions on the representativeness of the propulsive factors are presented in Section 5, and the conclusions are summarized in Section 6.

2. Vessel and propulsion system

The studied propulsion system is that of a twin-skeg 120 m research vessel. The vessel is equipped with an integrated rudder bulb-propeller hubcap system, where the rudder is slightly twisted. The hull characteristics are provided in Table 1, the hull is shown in Fig. 1, and the stern of the vessel, including propeller A and rudder, in Fig. 2. In the model-scale tests, conducted at the large towing tank at HSVA (scale factor 1:20.93), the hull can be considered hydraulically smooth apart from that turbulence was triggered using a 50 mm wide sandpaper-stripe with its front located $0.1L_{PP}$ (Length between perpendicular) downstream the forward perpendicular. In ship-scale a clean anti-fouling coated hull is assumed. One operating condition is considered in the study, the design point of the vessel, $V_S = 13$ knots corresponding to 1.462 m/s in model-scale. In model-scale the testing conditions are replicated while in ship-scale optimal trial conditions are assumed, i.e. no apparent wind, incoming waves or currents. The water properties for model-scale is corresponding to the model-test conditions: fresh water at 13.7 °C for the bare hull and self-propulsion simulations, and fresh water at 16.8 °C for the propeller open water simulations. In ship-scale sea water at 15 °C is assumed.

Model-scale test data is available for propeller A, an ice-classed propeller (Polar Class 5) heavily unloaded at the tip to minimize pressure pulses and cavitation nuisance. The two other propellers, B and C, are designed for this CFD study and never build or tested. Both has a more conventional radial load distribution, propeller B is ice-classed (also Polar Class 5) and propeller C is not. All propellers are 5-bladed controllable pitch propellers (CPP) with a propeller diameter (D_P) of 4.5 m, hub diameter (D_H) of 1.57 m, and expanded blade area ratio of 0.53. Their pitch to diameter ratios at $r/R = 0.7$ differs slightly, $P/D_{r/R=0.7} = 1.042$ for propeller A and $P/D_{r/R=0.7} = 1.014$ for propeller B and C, which is due to the differences in pitch distribution. The blades for all three propellers are depicted in Fig. 3.

Table 1
Main characteristics of hull.

	Ship-scale	Model-scale
L_{PP} [m]	120.28	5.7468
Breadth [m]	24	1.1467
Total displacement [m^3]	15 201	1.6579
Block coefficient	0.7502	0.7502
Nominal draught [m]	7	0.334

3. CFD method

Both model- and ship-scale CFD are conducted for: (1) Propeller in open water, (2) Bare hull and (3) Self-propulsion. This section first describes the general characteristics of the computational method, in common for all simulations, and thereafter focuses on the propeller open water, bare hull, and self-propulsion setups, respectively. Finally, the details concerning the computational grids are described.

3.1. Computational method

The commercial CFD package STAR-CCM+ ver. 2019.3 (Siemens P.L.M. Software, 2019), a finite volume method solver, is employed. STAR-CCM+ is set up to solve the conservation equations for momentum, mass, and turbulence quantities using a segregated solver based on the SIMPLE algorithm. For the propeller in open water the steady RANS equations are solved, while for the bare hull and complete vessel the unsteady RANS equations are required. A second order upwind discretization scheme in space is used and a second order implicit scheme for time integration.

Turbulence is modelled using SST $k-\omega$ (Menter, 1994; Menter et al., 2003) with Quadratic constitutive relations (QCR) (Spalart, 2000) and curvature correction (Arolla and Durbin, 2013; Siemens P.L.M. Software, 2019). In model-scale, the laminar to turbulent transition is modelled using the $\gamma - Re_\theta$ transition model (Langtry et al., 2006; Menter et al., 2006) including the cross-flow term (Langtry et al., 2015). The empirical "free-stream edge" is defined at 1.7 mm distance from the solid walls, the distance is not optimized for the hull, but it is of less importance since turbulence on the hull is triggered by the sandpaper-stripe modelled with surface roughness in CFD. In ship-scale the boundary layers are assumed fully turbulent and a transition model is not applied. In model-scale the boundary layers are resolved down to the wall, while in ship-scale wall functions are applied to model the boundary layers.

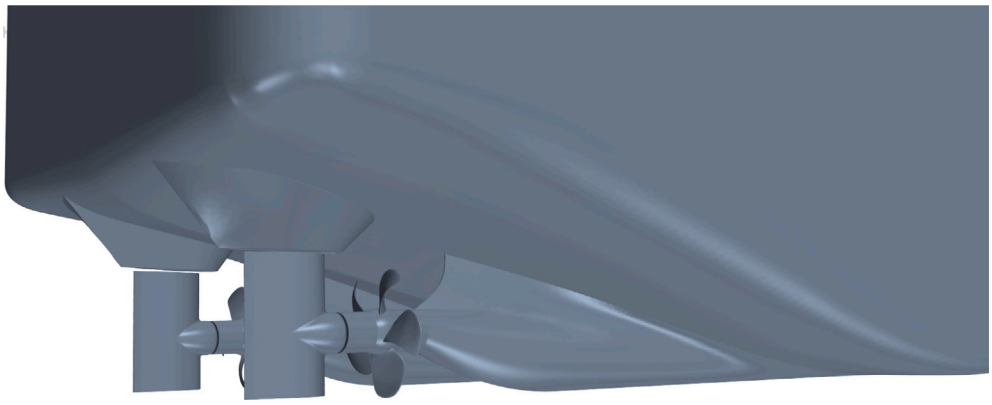

Fig. 2. Aft-ship geometry.

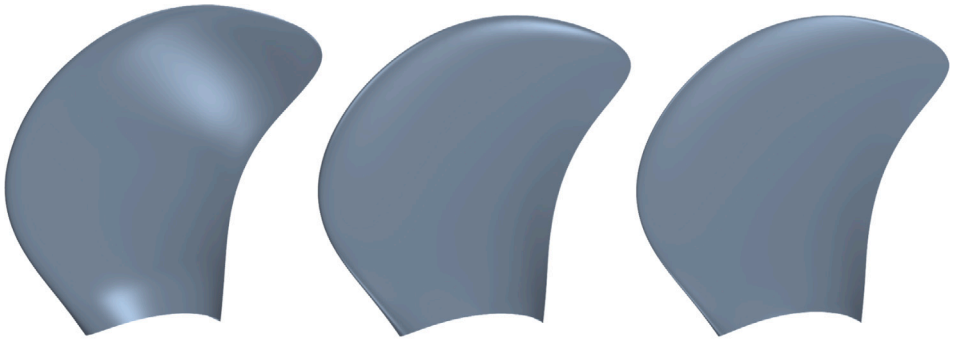

Fig. 3. Suction side view of propeller A (left), propeller B (centre), and propeller C (right).

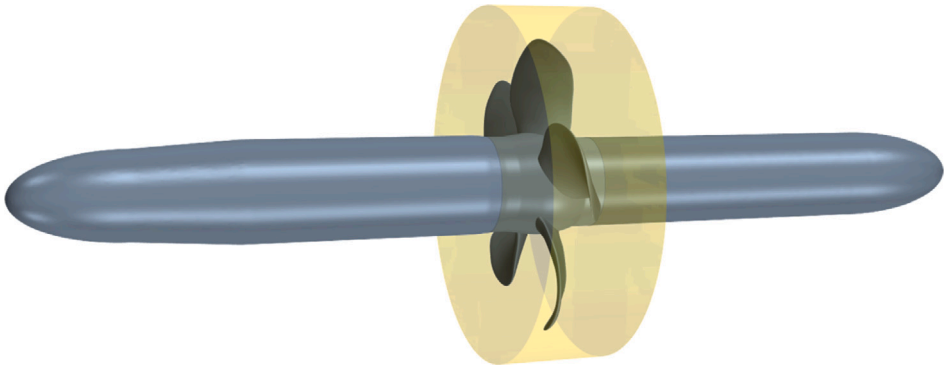

Fig. 4. Propeller attached to a streamlined cylindrical body. Propeller domain highlighted.

3.2. Propeller in open water

The propeller is mounted on a streamlined cylindrical body, to mimic the boundary layers close to the propeller hub during model tests, see Fig. 4. The computational domain is divided into a propeller domain, shown in Fig. 4, and an outer domain extending $6D_P$ upstream and downstream the propeller and with a diameter of $10D_P$.

The advance velocity (V_A) is set on the inlet boundary to reach the desired advance ratios ($J = V_A/nD_P$). The propeller rotation rate (n) is set to 26 rps, in line with available model test data. In ship-scale it is set to 94.2 rpm, similar to the ship-scale self-propulsion rotation rate. The inlet turbulence intensity and turbulent viscosity ratio are set to 5% and 10, respectively. The turbulence intensity represents the general turbulence level, here defined based on the turbulent kinetic energy, and the turbulent viscosity ratio is the ratio between the turbulent and molecular viscosity. In addition, for the model-scale setup, a turbulent kinetic energy source term is present from the inlet to the axial distance $0.6D_P$ in front of the propeller, to reduce the dissipation of turbulence from the inlet to the propeller. The resulting turbulence intensity just ahead of the propeller is about 2%. On the outlet boundary, a static pressure is prescribed, while the far field lateral boundary is modelled as a symmetry plane. Multiple Reference Frames (MRF) with frozen rotor interfaces are applied, where a rotating reference frame is specified for the propeller domain and a stationary reference frame for the outer domain.

3.3. Bare hull

Bare hull simulations are carried out both with the free surface modelled using the Volume-of-fluid (VOF) method and the hull free to heave and pitch, as well as with a symmetry plane representing the free surface (referred to as double-body model). In the second case the hull is locked in the obtained position from the free surface model. The resistance of the free surface model is used for the following analysis

of propulsive factors while the difference in resistance between the free surface and double-body model is assumed to represent the wave-making resistance also for the self-propulsion simulations, which are based on double-body models. It is admitted that the wave-making resistance most probably is influenced by the action of the propeller and that this assumption may have an impact on the analysis, on the other hand it reduces the required computational resources significantly, at the same time as it removes a lot of oscillations in resistance related to the wave making, complicating the analyses of small differences between the propulsion systems. This simplification is discussed further in Section 4.

The size of the computational domain for the bare hull simulations, given in [x, y, z] where x is the longitudinal and z the vertical directions, is [-3.5L_{PP}:2.5L_{PP}, 0:2L_{PP}, −1.5L_{PP}:1L_{PP}] ([0,0,0] located at mid-ship). This implies that only a half hull is modelled with a symmetry boundary condition at $y = 0$. For the double-body model the free surface is represented by a horizontal plane with symmetry boundary condition located at z = 0. An inlet velocity boundary condition of 1.462 m/s (model-scale) and 6.688 m/s, i.e. 13 knots, (ship-scale) is specified at the inlet and lateral boundaries. The inlet turbulence intensity and turbulence viscosity ratio are set to 1% and 10, respectively. These figures are of less importance for the $\gamma - Re_\theta$ transition model since the laminar-turbulent transition on the hull is controlled by the sandpaper-stripe. On the outlet, a hydrostatic pressure is prescribed for the free surface setup, where gravity is accounted for, and a uniform static pressure for the double-body model. For the free surface setup, the water surface level is initialized as the declared draft of the hull. The time step is set so it on average takes 200 time steps for a fluid particle to pass the hull.

The model-scale hull is modelled as a smooth wall, except the area covered with a 50 mm wide sandpaper-stripe to trigger turbulence. To ensure turbulent boundary layers downstream of the sandpaper-stripe when employing the $\gamma-Re_\theta$ transition model, this surface is modelled as rough, using the default roughness model implemented in STAR-CCM+ for low-Reynolds number turbulence models (Siemens P.L.M. Software, 2019) and an equivalent sand grain roughness (k_s) of 300 μm. This roughness height was found appropriate to trigger turbulence, but it is not investigated to which extent it is a correct physical representation of the sandpaper-stripe.

In ship-scale the hull is modelled as a rough wall. A clean anti-fouling coated hull is assumed, but the detailed roughness characteristics of the hull surface as build are unknown, so also the level of other surface imperfections such as weld seams, etc. It is assumed that the roughness can be modelled using a Colebrook/Grigson-type of roughness-function, $\Delta U^+ = 1/\kappa \cdot \ln(1 + k^+)$. Two different roughness levels are assumed to investigate the sensitivity to varying roughness, k_s = 5 μm and 27 μm. The first value is selected based on data in Andersson et al. (2020), but in the upper range for similar surfaces motivated by that some margin for surface imperfections are accounted for. The second value, k_s = 27 μm, is estimated based on reverse engineering to better replicate the ship-scale predictions by the test institute.

For the free surface model, the surface is modelled using the VOF method, implying that the domain consists of one fluid whose properties vary according to the volume fraction of water/air. The convective term is discretized using the High Resolution Interface Capturing (HRIC) scheme. The heave and pitch motions are modelled with the DFBI Equilibrium model in STAR-CCM+, implying that the model moves the body stepwise to obtain balanced forces and moments without solving the equations of motions.

3.4. Self-propulsion

The computational details described for the bare hull are valid also for the self-propelled hull. For the self-propulsion analyses the free surface is not modelled, instead a symmetry plane is applied. The inlet velocity is kept fixed and the propeller rotation rate adjusted to meet a fictive tow force, accounting for the additional resistance caused by wave making, not modelled in the self-propulsion CFD, and in model-scale also accounting for the rope force compensating for the high viscous resistance of the model. The propeller rotation is simulated applying sliding meshes with a time step corresponding to 1° propeller rotation.

In model-scale, the average tow force aimed for is the rope force used in the experimental test for propeller A complemented with the force difference between a free surface and a double-body model for the bare hull. In ship-scale, equilibrium is assumed, which implies that the fictive tow force aimed for is the force difference between a free surface and double-body model for the bare hull in ship-scale. The rotation rates of the propellers are adjusted manually to meet this tow force and obtain comparable results for the different propellers. All overall values are calculated as the average value for the last five propeller revolutions.

3.5. Computational grids

The computational grids are generated using STAR-CCM+ v2019.3. For the propeller domain polyhedral cells which are suitable for geometries with highly curved surfaces, are employed. Prism layers are extruded from the polyhedral surface mesh using the "Advancing Layer mesher" in STAR-CCM+. In model-scale, the boundary layer resolution on the propellers are adapted for the use of the $\gamma-Re_\theta$ transition model, which implies well resolved boundary layers in all three directions. 45 prism layers are applied near the walls with an expansion ratio of 1.1 and a near wall cell height of 2 μm, resulting in average $y^+ < 0.4$. The target cell size on the blades is set to 0.005D_P and the minimum cell size to 0.0005D_P. See Fig. 5 for a sectional cut of the model-scale propeller grid, focusing on the leading edge. In ship-scale, wall functions are applied to model the boundary layers, resolved using 20 prism layers with an expansion ratio of 1.2 and a total prism layer thickness of 0.01D_P. The resulting y^+ is in average 60. Grid sensitivity analyses of the propeller grid in model-scale shows that a refined grid with cell sizes about 25% smaller than the applied grid (total propeller domain cell count increased with about 60%) predicts 0.1% higher efficiency at $J = 0.7$. Numerical errors of that order of magnitude are considered acceptable, considering that grid convergence when applying a transition model is more difficult, and refining the grid further would imply an unacceptable computational cost.

The bare hull domain and outer domains for the propeller open water and self-propulsion setups, consists of predominantly hexahedral cut-cells, created using the "Trimmer mesher" in STAR-CCM+. In model-scale, were the boundary layers are resolved down to the wall, 29 prism layers with an expansion ratio of 1.25 is applied below the water surface, resulting in y^+ below the surface of about 0.25. Note that the grid on the hull is not adapted to the use of the transition model, this is not necessary since the location of the laminar-turbulent transition on the hull is controlled by hull roughness. In ship-scale, wall functions are applied to model the boundary layers on the hull and rudder, using 21 prism layers with an expansion ratio of 1.2, implying average y^+ around 200. Except for the prism layers, identical grid parameter settings are applied for model and ship-scale, with the reference cell size scaled according to the geometrical scaling of the vessel. Volumetric refinements are used around bow and stern, and for the free surface simulations anisotropic cell refinements are used around the free surface. Grid sensitivity analyses are conducted for the bare hull double-body model in model-scale and shows a minor (<0.1%) influence on resistance with a refined grid (all targeted sizes reduced by 25%). An additional grid sensitivity analysis was also conducted for the self-propulsion case, where the cell size of the refinement region around the propulsion system was reduced by a factor of 2; this had a negligible influence (<0.2%) on the overall variables. The grid (sectional cut and wall-surface grid) in the region surrounding the propulsion system is shown in Fig. 6. Table 2 summarizes the number of cells for each domain.

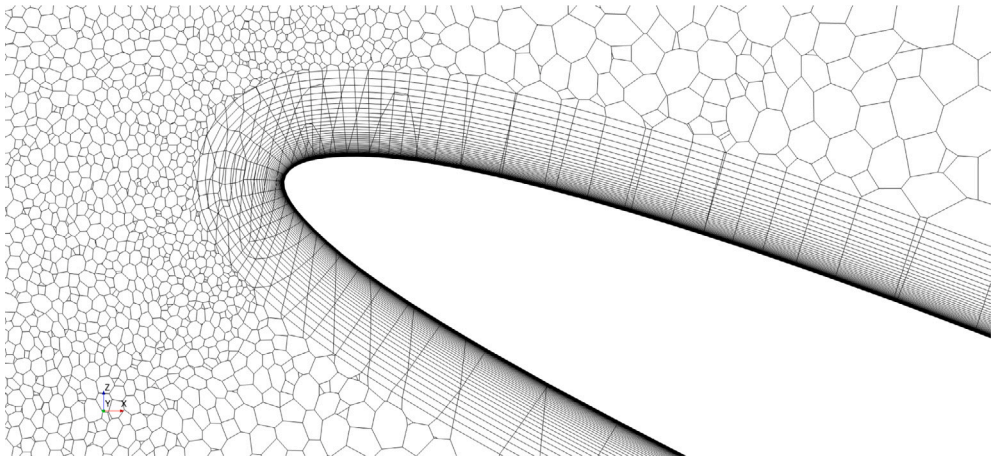

Fig. 5. Sectional cut ($0.7D_P$) of model-scale propeller grid.

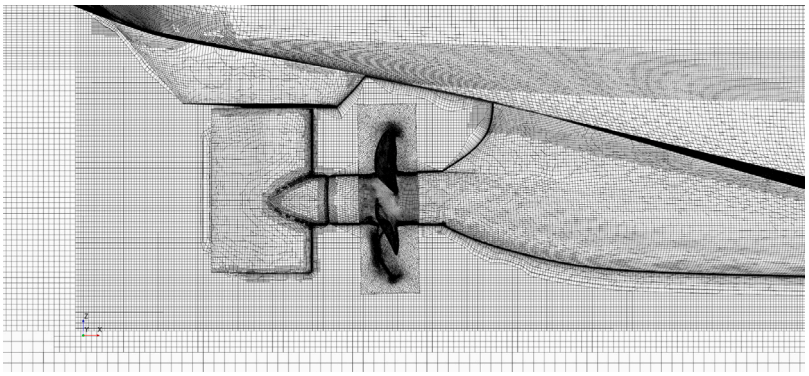

Fig. 6. Sectional cut and wall-surface grid in the propulsion system region.

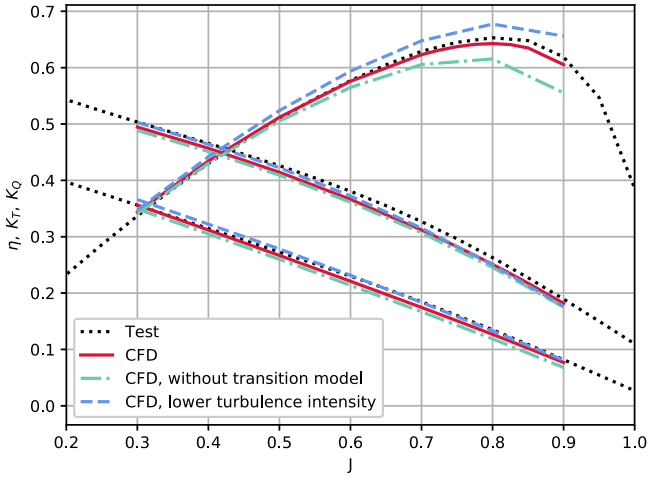

Fig. 7. Propeller A, model-scale test data vs. CFD predictions.

4. Validation of CFD-model

For the propeller in open water the available experimental data is thrust coefficient ($K_T = thrust/\rho n^2 D_P^4$), torque coefficient ($K_Q = torque/\rho n^2 D_P^5$) and efficiency ($\eta_O = J/2\pi \cdot K_T/K_Q$) for a range of advance ratios. This data is shown together with the CFD predictions in Fig. 7.

The difference between CFD and test at for instance J = 0.7 is −5.4% for K_T, −4.6% for K_Q and −0.9% for η (0.6%-points), so both K_T and K_Q are under-predicted in relation to test, but the relation between them, i.e. the efficiency, is more similar to the measured data. Fig. 7 also includes CFD-results without transition modelling, i.e. fully turbulent boundary layers assumed, and CFD results with the turbulence intensity just ahead of the propeller being about 0.5%. These CFD-results illustrate that despite model-scale Reynolds number (based on chord-length at $0.7D_P$, J = 0.7) of 755 000, the boundary layers in the test are most probably to some extent laminar, and also that the $\gamma - Re_\theta$ transition model is very sensitive to turbulent intensity. However, putting further efforts into improving the transition modelling is not considered worthwhile based on this case since detailed experimental data of the laminar to turbulent transition, such as paint-streak tests, are not available.

Table 2
Cell count for computational grids.

	Model-scale	Ship-scale
Propeller	$18.9{\cdot}10^6$	$9.6{\cdot}10^6$
Open water, outer domain	$2.5{\cdot}10^6$	$2.5{\cdot}10^6$
Bare hull, free surface	$24.4{\cdot}10^6$	$21.2{\cdot}10^6$
Bare hull, double-body model	$18.2{\cdot}10^6$	$15.6{\cdot}10^6$
Self-propulsion outer domain, double-body model	$18.1{\cdot}10^6$	$15.5{\cdot}10^6$

The predicted bare hull resistance correlates well with measured data with a deviation of −0.3%. Experimental wake measurements are only available at a lower speed, corresponding to 11 knots. CFD-results at model-scale velocity corresponding to 11 knots, both with a free-surface and double-body model, are shown in Fig. 8, together with experimental data. The differences in nominal wake between the two modelling approaches are minor, however compared to experimental

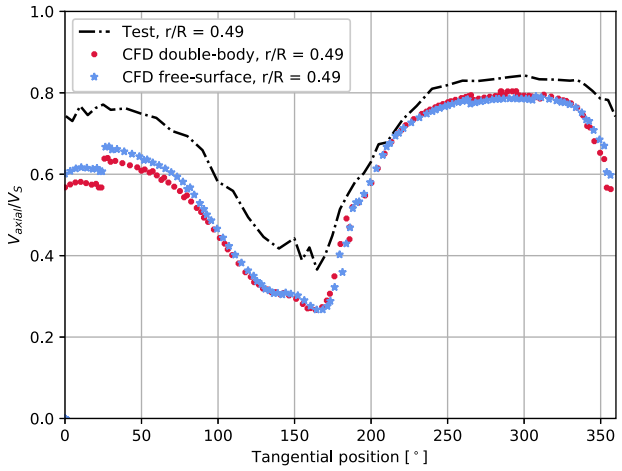

(a) r/R = 0.49

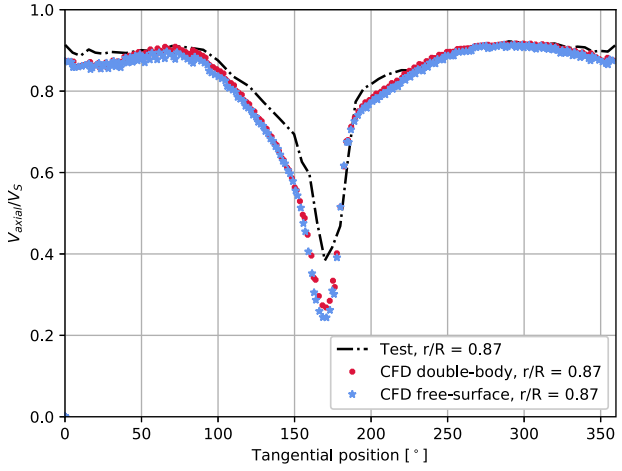

(b) r/R = 0.87

Fig. 8. Normalized axial velocity at propeller plane.

Table 3
Self-propulsion overall variables for Propeller A, model-scale test vs. CFD.

	Model-scale test	CFD
n [rps]	7.05	7.0388 (−0.2%)
K_T	0.1781	0.1712 (−3.9%)
K_Q	0.03165	0.03177 (0.4%)
Tow force [N]	15.08	15.12 (0.3%)
Power [W]	63.96	63.91 (−0.1%)
t	0.160	0.128 (−20.1%)
w_T	0.261	0.268 (2.9%)
η_H	1.136	1.191 (4.8%)
η_R	1.007	0.969 (−3.9%)
η_O	0.633	0.624 (−1.4%)

data the predicted velocities are lower, which especially is noted at lower radius and at the wake peak.

Table 3 includes a comparison of the self-propulsion overall variables and propulsive factors for CFD and experimental data. Note that the experimental propulsive factors are directly based on the measured data (i.e. not extrapolated to ship-scale as commonly seen in model test reports) to facilitate direct comparison with the CFD-results. All propulsive factors are evaluated using K_T-identity.

The power and rotation rate are predicted well by CFD, however the accordance between measured and CFD-predicted thrust is worse. As described above, the difference in bare hull resistance between the free surface and double-body model is assumed to represent the wave-making resistance also for the self-propulsion simulations. To examine if this assumption may be causing the deviation in predicted thrust, an additional self-propulsion CFD is setup applying VOF to represent the free surface. As suspected, the resistance, and hence tow force are oscillating to such a degree that it would make these results difficult to apply for the comparisons in Section 5 and the required computational resources are significantly higher, mainly due to that the physical time needed to be simulated increases to achieve converged results. The results indicate that only a small fraction (about 20%) of the deviation in thrust may be explained by the wave-making resistance simplification (i.e. that it is the same as for the bare hull). Further, the self-propulsion CFD-results with a free surface shows that the propulsive factors agree very well with the double-body model results. Another possible explanation for the thrust deviation may be that the hull/rudder resistance is not influenced to the same degree by the action of the propeller in CFD as in model test, i.e. that the physical modelling introduced in the CFD is not good enough to capture these interactions. A third possible reason may be that the way the thrust is evaluated in test and CFD differ, i.e. the integration of surface forces in the CFD compared with the gauges in the experiment.

CFD predicts $\eta_R < 1$, i.e. showing that the propeller at identical K_T has a lower K_Q in open water than in self-propulsion, while the opposite holds for the model test. It may partly be explained by the nominal wake predicted by CFD deviating slightly from test (as shown in Fig. 8), in addition there is always a risk for a modelling error due to differences in set up and/or evaluation. Further it is strongly suspected that possible reasons to the deviations between CFD and model test data is both transition and general turbulence modelling.

The aim of this study is to understand the interaction effects for the different propulsion systems, is it possible with this accuracy of the self-propulsion CFD? It is not unquestionable, however our belief is that although we do not capture all effects seen in the tests good enough, it should be expected that the different propellers suffer similarly. Unfortunately, there is no clear way forward to improve the CFD-modelling since the extent of the laminar boundary layers on the propeller are unknown in a self-propulsion test. Unlike propeller open water tests where the extent of the laminar boundary layers and laminar to turbulent transition can be studied using paint-streaks (see for instance Bhattacharyya et al. (2015) or Li et al. (2019)), it is difficult to conduct such studies in-behind conditions due to the strong tangential variation in the flow field. This is not only an issue within this study, but generally holds for all model-scale CFD-validation of detailed propeller-performance in-behind conditions. However, since it neither is possible to conduct detailed studies of propeller-hull interaction based on model-tests (flow details cannot be extracted to the extent required) this study will be based on CFD which is considered to be the best available alternative, keeping in mind that the CFD-results contain these issues.

5. Results and discussion

A self-propulsion comparison based on overall variables, as commonly presented for a model-scale test, is included in Section 5.1. However, to move beyond this traditional characterization of propulsion system performance and better understand the propeller-hull interaction effects, further analyses of the results and possible post-processing alternatives are included in Section 5.2. Finally, in Section 5.3 it is discussed to what extent the model scale propulsive factors are representative to use in the scaling procedure.

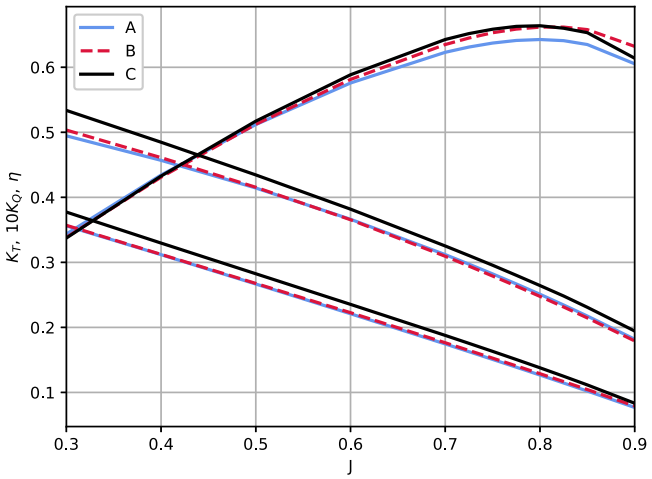

Fig. 9. Model-scale CFD results for the propellers in Open Water.

Table 4
CFD-predicted self-propulsion overall variables and propulsive factors in model-scale.

Propeller	A	B	C
n [rps]	7.0388	6.9570	6.8674
Thrust [N]	36.22	36.06	36.08
K_T	0.1712	0.1745	0.1792
K_Q	0.03177	0.03190	0.03253
Tow force [N]	15.12	15.12	15.09
Power [W]	63.91	61.97	60.78
t	0.128	0.124	0.123
w_T	0.268	0.278	0.275
η_H	1.191	1.214	1.210
η_R	0.969	0.962	0.968
η_O	0.626	0.638	0.649

5.1. Propulsion system performance in model and ship-scale

The model-scale performance of the three propulsion systems, as predicted by CFD, are presented in Table 4. As expected, the least power is required by the propeller without ice-class, propeller C, which has a slender blade profile, followed by propeller B and A. The results are in line with the open water efficiency of each propeller at the average loading, propeller C having the highest open water efficiency, followed by propeller B and A. The model-scale open water characteristics for the three propellers obtained from CFD are shown in Fig. 9. However, if studying the self-propulsion results in more detail it is noted that the differences in η_O and delivered power are not the same. For instance, η_O for propeller B is 1.9% higher than for propeller A, while the required power for propeller B is 3% lower. Between propeller B and C the differences are less, propeller C has 1.7% higher η_O while it requires 1.9% less power in-behind. These differences are commonly explained using the propulsive factors. Here it can for instance be noted that η_H is 1.9% higher for propeller B than A and that η_R is 0.7% lower; but what does that really mean, what are causing these differences?

Before investigating the model-scale propeller-hull interaction effects further the overall results and propulsive factors for ship-scale self-propulsion are presented in Table 5. Also propulsive factors based on ship-scale open water and bare hull CFD are included. All ship-scale results presented are for the rougher surface, $k_s = 27$ μm, this hull state requires about 2% more power than the smoother surface. The relative differences between the propulsion systems are very similar for the two roughness conditions, and notable is also that η_R remains almost unchanged.

Also the results in ship-scale shows that the least power is required by propeller C, followed by propeller B and A, which as well is expected based on ship-scale open water efficiency of each propeller at the average loading in-behind. However, the relative differences also in ship-scale are not the same: η_O for propeller B is 1.2% higher than for propeller A, while it requires 2.1% less power in-behind conditions. Also when comparing propellers B and C differences are noted that need to be explained: η_O is 2.4% higher for propeller C than for propeller B, but the difference between required power in-behind is only 1.2%.

Table 5
CFD-predicted self-propulsion overall variables and propulsive factors in ship-scale.

Propeller	A	B	C
n [rpm]	95.51	95.59	94.10
Thrust [kN]	356.1	354.1	353.8
K_T	0.1670	0.1658	0.1709
K_Q	0.0297	0.02900	0.03002
Tow force [kN]	−0.42	0.10	0.03
Power [kW]	2850	2790	2755
t	0.113	0.109	0.108
w_T	0.226	0.225	0.222
η_H	1.146	1.149	1.146
η_R	0.996	1.001	0.993
η_O	0.649	0.657	0.672

5.2. Propeller-Hull interaction effects

The operating conditions for the propeller blade varies significantly within the wake, both tangentially and radially, due to the wake field. In Fig. 10, nominal axial velocities (normalized) at the propeller plane are shown for both model and ship-scale. In addition to the axial variations, the tangential and radial velocity components are critical for blade loading, these are illustrated by the vectors in Fig. 10. The transverse velocity field is dominated by the positive vertical component, a consequence of that flow follows the buttock lines of the aft-ship. In Fig. 11, K_Q for one blade around a revolution is shown. 0° corresponds to the top position and the high torque noted at about 345° is the wake-peak, i.e. the region of largest velocity deficit in the wake, and then at about 90°-110°, a second lower flat peak is observed when the blade rotates down, meeting the upwards directed flow, resulting in high angles of attack. Thereafter the load decreases with a minimum at about 270° when the propeller blade rotates with the upward directed flow and the angles of attack are at its lowest level.

Propeller performance is commonly evaluated in terms of efficiency, which for a propeller is defined as advance velocity times the propeller thrust divided by the delivered power to the propeller. Since an advance velocity cannot clearly be defined for a propeller in-behind conditions another performance measurement is required. In the ITTC-1978 performance prediction method ITTC (2017) the decomposition into η_H, η_R, and η_O is applied for scaling purposes, and these factors are also commonly used to describe the propulsion system interaction effects, however, using CFD other possibilities are available. A common measure for an airfoil is the lift to drag ratio (L/D). Transformed to the coordinate system commonly applied for a marine propeller, it corresponds to thrust over torque divided by radius, which is the same as K_T/K_Q. A great benefit with such a measure is that it can be evaluated at each tangential position of the blade in the wake, both for the whole blade or extracted for radial blade sections, to better understand the propeller performance in-behind conditions. Figs. 12 and 13 displays this ratio for the blades of the three propellers in model and ship-scale. These plots are naturally influenced by differences in propeller performance in homogeneous inflow, i.e. open water, however two distinct observations are made: (1) the propeller A blade has lower K_T/K_Q, i.e. is performing worse, than the other two propellers after the wake peak, between about 0 and 150°; (2) the propeller C blade has lower K_T/K_Q, i.e. is performing worse, than the other propellers at minimum load, around 270°.

Focusing first on observation (1), the degradation of performance of propeller A, the radial K_T/K_Q-distributions are plotted for blade A and

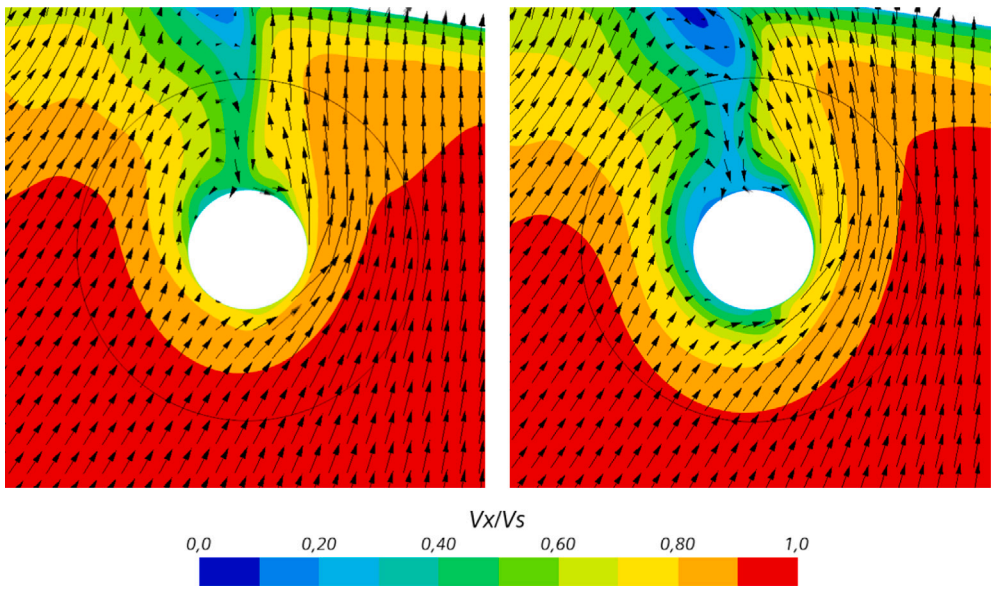

Fig. 10. Contour plots of nominal axial velocity (axial velocity normalized with V_S) with vectors for transverse velocities at propeller plane in ship-scale (left) and model-scale (right).

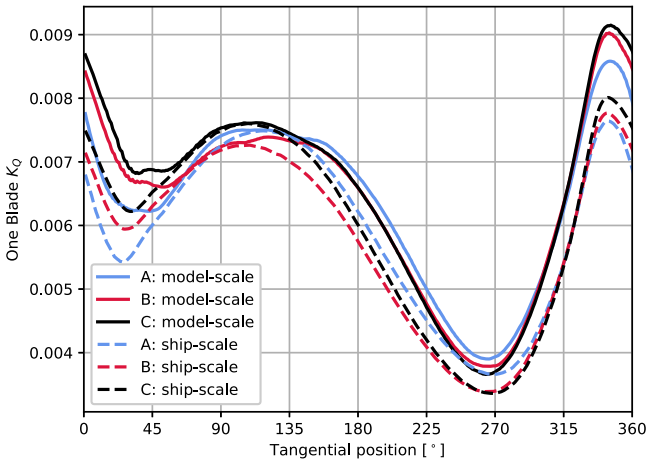

Fig. 11. CFD results for K_Q variation in the wake.

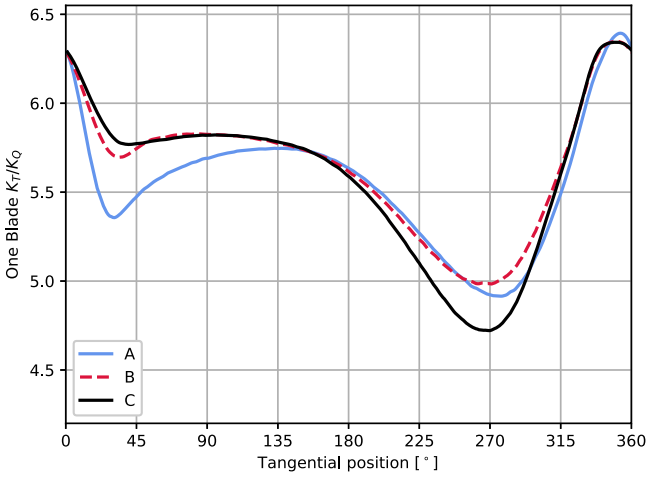

Fig. 13. Ship-Scale CFD results for K_T/K_Q variation in the wake.

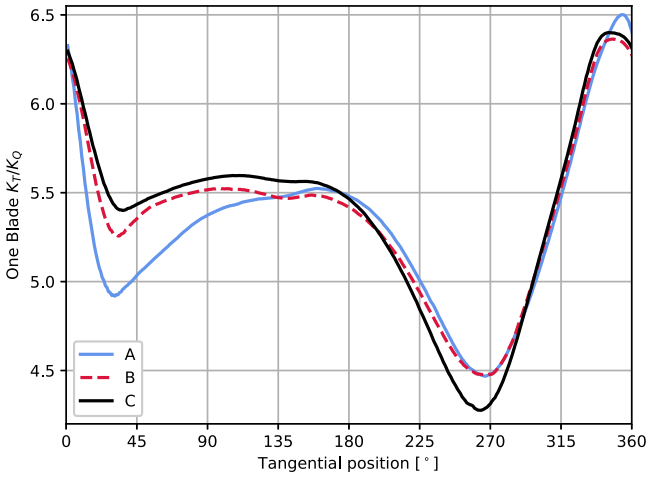

Fig. 12. Model-Scale CFD results for K_T/K_Q variation in the wake.

B in the wake at 40° as well as in open water at self-propulsion average K_T in Fig. 14. The results are for model-scale with open water results at the same Reynolds number as the self-propulsion case, however the same trend is present in ship-scale. It is noted that the load shift caused by the wake, with lower axial velocities towards the hub and higher axial velocities at outer radius, results in higher K_T/K_Q towards the hub and lower towards the tip, which holds for both propellers in relation to open water. Further, it is clearly seen that the degradation of performance of propeller A is due to poor performance of the tip, which even has a negative K_T/K_Q, due to negative thrust. The profile towards the tip of the heavily tip-unloaded propeller A has obviously a negligible camber and at some sections of the wake, such as around 40°, it also experiences negative angles of attack. Coupling it to a common propeller open water diagram, it could be explained as if the tip operates to the right of the efficiency peak with low or negative thrust and with the required torque dominated by shear stresses. A question arising is why this large difference between the propellers is seen in the low load region after the wake peak, but not at minimum load around 270°? The explanation, specific for this case, is that it seems like the propeller B tip performs well after the wake peak, however when

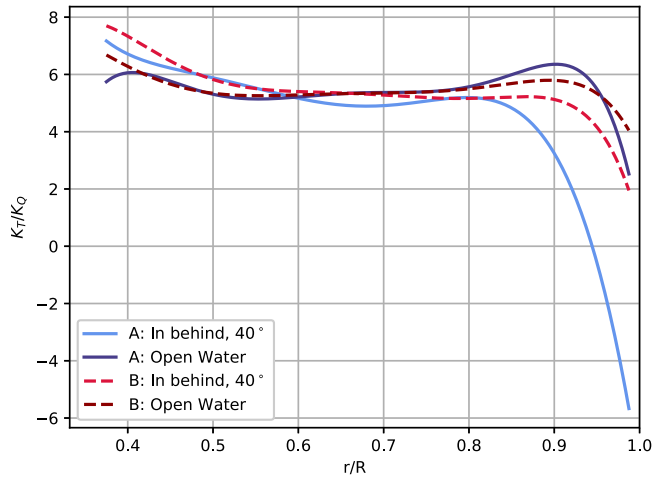

Fig. 14. Model-Scale CFD results for radial variation of K_T/K_Q at the tangential position 40°. Open water at self-propulsion average K_T.

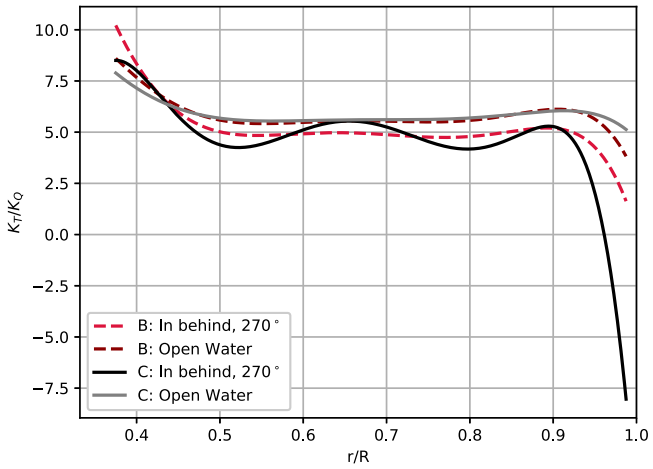

Fig. 15. Ship-Scale CFD results for radial variation of K_T/K_Q at the tangential blade position 270°. Open water at self-propulsion average K_T.

the load reduces further, such as around 270°, the performance of the propeller B tip also falls drastically. Differences in performance around minimum load also has less impact on the overall variables, since the fraction of the total thrust and torque produced in this section of the wake is low.

Shifting focus to the second observation in Figs. 12 and 13: that propeller C is performing worse than the other propellers at minimum load. In Fig. 15, the radial K_T/K_Q-distributions are evaluated for blade B and C in the wake at 270° as well as in open water. The results are shown in ship-scale, but the same trend is present in model-scale. An inferior performance is noted towards the tip for propeller C in the wake at 270°, a position where the blade section is experiencing a very low load and even negative angles of attack, due to a combination of higher axial velocities at outer radii and blade rotation aligned with the upwards directed flow. The contour plots in Fig. 16, shows a radial cut at r/R=0.9 for both propeller B and C at 270°. At this section the angles of attack are negative, which is indicated by the stagnation point location. For propeller C the flow cannot follow the sharp leading edge of the profile onto the pressure side, which is evident from the low velocities just downstream the leading edge. This flow behaviour results in an even lower pressure on the pressure side, compared to what is noted for propeller B. The blunter leading edge of propeller B is capable of maintaining an attached flow even at this angle of attack. Further is this effect amplified by the lower rotation rate of propeller C in-behind since it implies even lower angles of attack, i.e. more negative. In Figs. 12 and 13 it can be observed that the differences between the propellers are slightly smaller in model-scale, which partly may be explained by the larger wake field, and hence less operation at very low load. Finally, the superior performance of a blunt leading edge at low load can also explain why the efficiency peak of propeller A and B is noted at higher advance ratio in relation to propeller C, as seen in Fig. 9.

As earlier discussed, the propulsive factors evaluated in model-scale may also be influenced by differences in performance due to different Reynolds numbers of the open water and self-propulsion test. In this study, self-propulsion is conducted at a Reynolds number of about 200 000 and open water at about 750 000, in line with available model-test data for propeller A. In Fig. 17 the propeller efficiencies in open water are evaluated at J = 0.725, which is close to the self-propulsion average loading, for four different Reynolds numbers. The efficiency of propeller C is less reduces with reduced Reynolds number compared to the two ice-classed propellers. Studying the flow in more detail it is noted that the thicker profiles of propeller A and B are punished to a higher degree by the thicker boundary layers at lower Reynolds numbers. The differences are noted towards the trailing edge where a thicker profile is more prone to separation at the low Reynolds number. This effect, that a thicker profile implies higher scale effects on K_T and K_Q, is also incorporated in the common ITTC-78 scaling procedure for open water characteristics (ITTC, 2017).

In addition to evaluation of the blade performance in the wake and a sensitivity study to the open water performance at different Reynolds numbers, a CFD study of the interaction effects ought to be complemented with an investigation of thrust differences and what they stem from. As noted in Tables 4 and 5, these differences are small, especially they are negligible between propeller B and C which have the same radial load distribution. A slightly higher thrust, 0.3% and 0.6% for model and ship-scale respectively, is required by propeller A, which has a less even radial load distribution as a direct consequence of the tip-unloading, implying higher maximum load, and hence more uneven acceleration of the flow field, with higher maximal velocities. Propeller A causes an increased drag on the upstream hull, which needs to be compensated by a higher thrust.

5.3. Relating observed hydrodynamic details to the propulsive factors

So how are the interaction effects described above reflected in the traditional propulsive factors? Beginning with the thrust deduction, t, which is relatively straight forward since it actually only represent the differences in hull and rudder resistance with and without working propeller. There are only minor differences in thrust deduction between propeller B and C, which need to produce the same thrust, while it is slightly higher for propeller A, which needs to produce more thrust to compensate for the increased drag. These observations holds for both model and ship-scale, however the thrust deduction differs between the scales, being about 12% lower in ship-scale. It is not possible to draw any general conclusions from one specific case, but it is noted that the assumption that thrust deduction should be equal in model and ship-scale is not valid based on these CFD-results.

The Taylor wake fraction w_T is more problematic. Since all propellers have the same diameter, and B and C also the same radial load distribution, there are no reasons to expect differences in w_T if it only described the velocities in the propeller plane in relation to the ship speed. However, the Taylor wake fraction is obtained using K_T-identity which implies that differences in thrust and rotation rate, which is a consequence of the complete system performance, also matters for w_T. The differences in w_T between propeller B and C can act as a simple example: Both propellers produce the same thrust, but K_T differs since it scales the thrust with n^2. K_T-identity gives a corresponding

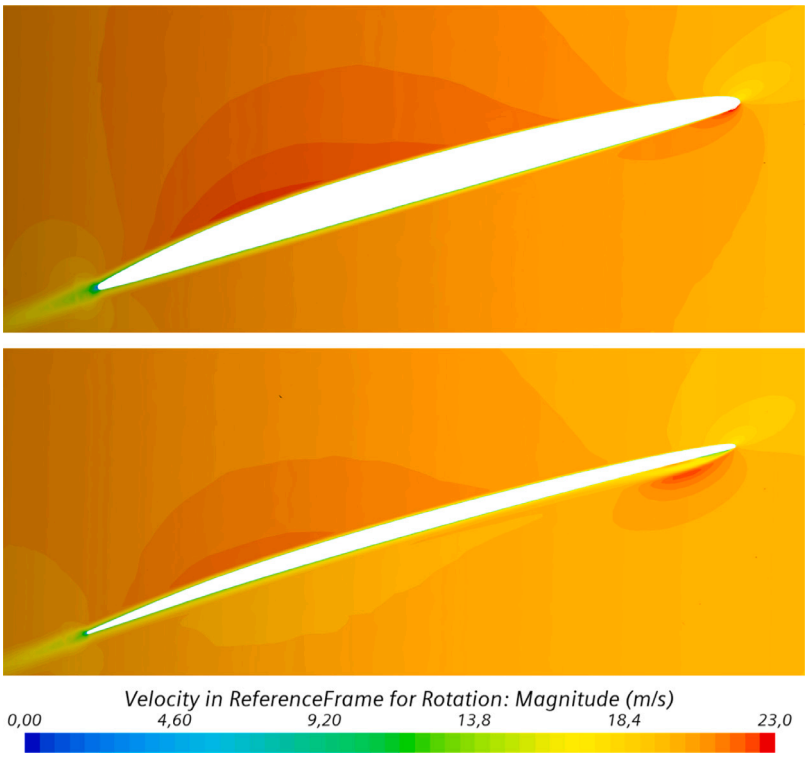

Fig. 16. Ship-Scale CFD results; contours of velocity magnitude in a reference frame rotating with the propeller at a radial section at r/R = 0.9. Propeller B (top) and propeller C (bottom).

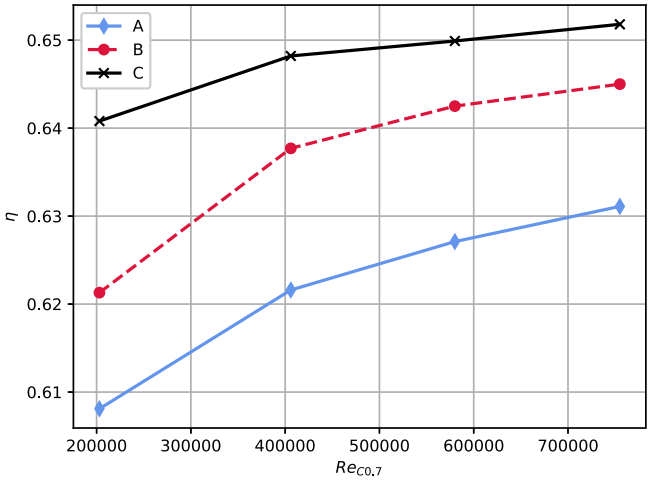

Fig. 17. Model-Scale CFD results; propeller open water efficiency versus Reynolds number.

J in open water, and to obtain V_A multiplication is done with nD, i.e. the difference in rotation rate enters as a difference in w_T (n^2/n). This shows that the Taylor wake fraction does not solely represent a wake velocity, but is also influenced by system performance. It proves as a good example on why it can be difficult to grasp differences in propulsive factors between different propulsion systems and also illustrates the complications with wake fraction scaling. It may be possible to scale the wake magnitude between two different Reynolds numbers, but it seems very complex to scale the part of the wake fraction associated with system performance in a fair manner.

Even more difficult to grasp is the hull efficiency η_H which is obtained from t and w_T. Since w_T is dependent on system performance, so is η_H. However, the observed differences in η_H between the systems are small, except for the configuration with propeller A in model-scale, when η_H is clearly lower than the other model-scale values.

The relative rotative efficiency, η_R is the ratio of $K_{Q,OW}/K_{Q,SP}$ at K_T-identity. For ship-scale were the fictive open water simulations are conducted at the same rotation rate as in-behind, it simplifies to $torque_{OW}/torque_{SP}$ at K_T-identity. In ship-scale, where differences due to varying Reynolds numbers between self-propulsion and open water tests can be neglected, the lower η_R of propeller A and C can most probably be linked to the poor tip performance at low load in-behind, caused by heavily unloading and a sharp leading edge, respectively. The model-scale η_R is a few percent lower than the ship-scale values, which can be explained by that K_Q is increasing with reduced Reynolds number and that the Reynolds number difference between self-propulsion and open water is not negligible. Fig. 17 shows that less scale effect on efficiency is noted for propeller C, with a lower thickness/chord ratio. The largest scale-effect is noted for propeller B, which also seems to be reflected in its low η_R. The relative differences between the values of η_R in model-scale indicates that the scale effect due to inconsistent Reynolds numbers in self-propulsion and open water seems to be of higher importance than the reduced performance of the propeller A and C tips. It should also be mentioned, as noted above, that the reduced performance of the propeller C tip may be of less importance in model-scale, due to the larger wake. Concluding this, if these CFD results are representative, model-scale η_R are not representative for ship-scale since it to a large extent is dependent on scale-effects between model-scale open water and self-propulsion Reynolds numbers, and also dependent on the model-scale wake. It shows the necessity to account for the Reynolds number differences between self-propulsion and open water tests in some manner. Further, it also motivates the need to increase our knowledge on the ship-scale wake, to learn more on the real propeller operating conditions, as well as possible differences between the wake in ship-scale and in and model-scale.

η_O represent propeller performance in homogeneous inflow. However, an important remark is that η_O are compared using K_T-identity,

and since K_T is scaled by the rotation rate (n^2) it implies that differences in loading (J) caused by rotation rate are also included. In other words, a better propulsion system, as for instance propeller C compared to propeller B, has the capability to produce the required thrust at a lower rotation rate and then further benefits from a higher efficiency. In ship-scale, at the same loading $J = 0.725$, propeller C has 1.5% higher efficiency than propeller B, while η_O in Table 5 indicate 2.4% difference. In other words, the interaction effects impact how η_O is evaluated, however it does not pose any problems for scaling.

6. Conclusions

Three separate methods are used to study the propeller-hull interaction effects: Evaluation of K_T/K_Q for a blade around a revolution and radial distributions of the same measure, open water performance dependency on Reynolds number and studies of reasons behind thrust/drag differences. Comparisons of K_T/K_Q at different tangential and radial positions are considered to be highly beneficial to understand the blade performance in the wake and could be applied for blade, as well as hull, design.

Based on this presentation of the CFD-results, four main observations regarding the propulsion system performance in-behind are made:

- Tip-unloading is deteriorating propeller performance to a larger extent in-behind conditions since the wake distribution further decreases the load on the blade tips.
- The blunter leading edge of an ice-classed propeller has a superior performance at low load in relation to a sharper leading edge, it is less sensitive to poor performance at negative angles of attack. This is beneficial in-behind conditions were the load is varying to a large extent.
- In model-scale the interaction effects are to a large extent influenced by scale-effects between self-propulsion and open water Reynolds numbers. It is noted that the performance of ice-classed propellers with thicker blade profiles degrades more at low Reynolds numbers.
- The hull drag is increasing more with a tip-unloaded propeller, hence a more even radial load distribution favour a low thrust deduction factor.

Even if there are doubts whether the CFD-results correctly predict all aspects of the flow around the self-propelled vessel, the analysis performed indicate that the propulsive factors as derived in model-scale are certainly questionable to use in the scaling procedure. Firstly since they to a large extent are influenced by scale-effects between self-propulsion and open water Reynolds numbers, and secondly since their association to the observed hydrodynamics makes the commonly applied scaling procedure of them doubtful. This study indicate that t is not the same in model and ship-scale as commonly assumed and since w_T is not only a measure of the wake velocity, but also influenced by propulsion system performance, a general and representative scaling procedure seems impossible. Further it is shown that η_R is not the same in model and ship-scale, as commonly assumed. η_R seems to be highly dependent on scale-effects between model-scale self-propulsion and open water Reynolds numbers, as well as on the model-scale wake. However, a final remark to make is that these conclusions are drawn based on one single vessel, and comparison of propellers with and without ice-class and tip-unloaded versus more conventional radial load distributions. For comparison of other propulsion systems, the representativeness of the propulsive factors may not need to be questioned.

To build up the knowledge further within the field of propeller-hull interaction, more detailed studies of the flow for various propulsion systems, in both model and ship-scale, going beyond the traditional propulsive factors, are required. This could both question and possibly improve the commonly applied scaling procedures and further provide a foundation for new standardized ways of analysing and presenting propeller-hull interaction based on CFD-results.

CRediT authorship contribution statement

Jennie Andersson: Conceptualization, Methodology, Validation, Formal analysis, Writing – original draft, Visualization, Project administration. **Robert Gustafsson:** Conceptualization, Methodology, Resources, Writing – review & editing, Supervision. **Rikard Johansson:** Conceptualization, Methodology, Writing – review & editing, Supervision. **Rickard E. Bensow:** Conceptualization, Methodology, Writing – review & editing, Supervision, Funding acquisition.

Declaration of competing interest

The authors declare that they have no known competing financial interests or personal relationships that could have appeared to influence the work reported in this paper.

Acknowledgements

This research is supported by the Swedish Energy Agency (grant number 38849-2) and Kongsberg Maritime Sweden AB through the University Technology Centre in Computational Hydrodynamics hosted by the Department of Mechanics and Maritime Sciences at Chalmers. The simulations were performed on resources provided by the Swedish National Infrastructure for Computing (SNIC) at the National Supercomputer Centre in Linköping (NSC) and at Chalmers Centre for Computational Science and Engineering (C3SE).

References

Andersson, J., Gustafsson, R., Eslamdoost, A., Bensow, R.E., 2018. On the selection of optimal propeller diameter for a 120 m Cargo vessel. In: SNAME Propeller-Shafting 2018 Symposium, Norfolk, Virginia, USA.

Andersson, J., Oliveira, D.R., Yeginbayeva, I., Leer-Andersen, M., Bensow, R.E., 2020. Review and comparison of methods to model ship hull roughness. Appl. Ocean Res. 99.

Arolla, S.K., Durbin, P.A., 2013. Modeling rotation and curvature effects within scalar eddy viscosity model framework. Int. J. Heat Fluid Flow 39, 78–89.

Bensow, R.E., 2015. Large eddy simulation of a cavitating propeller operating in behind conditions with and without pre-swirl stators. In: Proceedings of the 4th International Symposium on Marine Propulsors - SMP'15, Austin, Texas, USA.

Bhattacharyya, A., Neitzel, J.C., Steen, S., Abdel-Maksoud, M., Krasilnikov, V., 2015. Influence of flow transition on open and ducted propeller characteristics. In: Proceedings of the Fourth International Symposium on Marine Propulsors, Austin, Texas, USA.

Eslamdoost, A., Andersson, J., Bensow, R., Gustafsson, R., Hyensjö, M., 2017. Analysis of propeller-hull interaction phenomena on a self-propelled axisymmetric body. In: Proceedings of the Fifth International Symposium on Marine Propulsors, Espoo, Finland.

Hally, D., 2019. Energy balance analysis using RANS-BEM coupling. In: Proceedings of the Sixth International Symposium on Marine Propulsors, Rome, Italy.

ITTC, 2017. 1978 ITTC Performance prediction method. Recommended procedure 7.5 - 02 - 03 - 01.4 rev 04.

Langtry, R.B., Menter, F.R., Likki, S.R., Suzen, Y.B., Huang, P.G., Volker, S., 2006. A correlation-based transition model using local variables Part II: Test cases and industrial applications. J. Turbomachinery 128 (3), 423.

Langtry, R.B., Sengupta, K., Yeh, D.T., Dorgan, A.J., 2015. Extending the γ-Reθt local correlation based transition model for crossflow effects. In: 45th AIAA Fluid Dynamics Conference, Dallas, USA. pp. 1–12.

Li, D.-Q., Lindell, P., Werner, S., 2019. Transitional flow on model scale propellers and their likely influence on performance prediction. In: Proceedings of the Sixth International Symposium on Marine Propulsors, Rome, Italy.

Liefvendahl, M., Bensow, R.E., 2014. Simulation-based analysis of hull-propeller interaction for a single-screw transport ship. In: Proceedings of the 30th Symposium on Naval Hydrodynamics, Hobart, Australia.

Lücke, T., 2019. Particular model propeller behavior in EFD & CFD. In: Proceedings of the Sixth International Symposium on Marine Propulsors, Rome, Italy.

Menter, F.R., 1994. Two-equation eddy-viscosity turbulence models for engineering applications. AIAA J. 32 (8), 1598–1605.

Menter, F.R., Kuntz, M., Langtry, R., 2003. Ten years of industrial experience with the SST turbulence model. In: Hanjalic, K., Nagano, Y., Tummers, M. (Eds.), Turbulence, Heat and Mass Transfer 4. Begell House, Inc..

Menter, F.R., Langtry, R.B., Likki, S.R., Suzen, Y.B., Huang, P.G., Völker, S., 2006. A correlation-based transition model using local variables Part I: Model formulation. J. Turbomachinery 128 (3), 413–422.

Schuiling, B., van Terwisga, T., 2018. Energy loss analysis for a propeller operating behind a ship. In: 32nd Symposium on Naval Hydrodynamics, Hamburg, Germany.
Schuiling, B., Van Terwisga, T., 2017. Hydrodynamic working principles of energy saving devices in ship propulsion systems. Int. Shipbuild. Prog. 63 (3–4), 255–290.
Siemens P.L.M. Software, 2019. STAR-CCM+ Documentation version 2019.3.
Spalart, P.R., 2000. Strategies for turbulence modelling and simulations. Int. J. Heat Fluid Flow 21 (3), 252–263.
Voermans, A., 2017. Development of the Wärtsilä EnergoFlow: An innovative energy saving device. In: Proceedings of the Fifth International Symposium on Marine Propulsors, Helsinki, Finland.